ACS APPLIED MATERIALS & INTERFACES

Research Article

www.acsami.org

Synthesis of PCDTBT-Based Fluorinated Polymers for High Open-Circuit Voltage in Organic Photovoltaics: Towards an Understanding of Relationships between Polymer Energy Levels Engineering and Ideal Morphology Control

Jonggi Kim,[†] Myoung Hee Yun,[†] Gi-Hwan Kim,[†] Jungho Lee,[†] Sang Myeon Lee,[†] Seo-Jin Ko,[†] Yiho Kim,[†] Gitish K. Dutta,[†] Mijin Moon,[†] Song Yi Park,[†] Dong Suk Kim,[‡] Jin Young Kim,*[,†] and Changduk Yang*[,†]

[†]School of Energy and Chemical Engineering, KIER-UNIST Advanced Center for Energy, Low Dimensional Carbon Materials Center, Ulsan National Institute of Science and Technology (UNIST), Ulsan 689-798, Korea

[‡]KIER-UNIST Advanced Center for Energy, Korea Institute of Energy Research, Ulsan 689-798, Korea

Supporting Information

ABSTRACT: The introduction of fluorine (F) atoms onto conjugated polymer backbone has verified to be an effective way to enhance the overall performance of polymer-based bulk-heterojunction (BHJ) solar cells, but the underlying working principles are not yet fully uncovered. As our attempt to further understand the impact of F, herein we have reported two novel fluorinated analogues of PCDTBT, namely, **PCDTFBT** (1F) and **PCDT2FBT** (2F), through inclusion of either one or two F atoms into the benzothiadiazole (BT) unit of the polymer backbone and the characterization of their physical properties, especially their performance in solar cells. Together with a profound effect of fluorination on the optical property, nature of charge transport, and molecular organization, F atoms are effective in lowering both the HOMO and LUMO levels of the polymers without a large change in the energy bandgaps. **PCDTFBT**-based BHJ solar cell shows a power conversion efficiency (PCE) of 3.96 % with high open-circuit voltage (V_{OC}) of 0.95 V, mainly due to the deep HOMO level (−5.54 eV). To the best of our knowledge, the resulting V_{OC} is comparable to the record V_{OC} values in single junction devices. Furthermore, to our delight, the best **PCDTFBT**-based device, prepared using 2 % v/v diphenyl ether (DPE) additive, reaches the PCE of 4.29 %. On the other hand, doubly-fluorinated polymer **PCDT2FBT** shows the only moderate PCE of 2.07 % with a decrease in V_{OC} (0.88 V), in spite of the further lowering of the HOMO level (−5.67 eV) with raising the number of F atoms. Thus, our results highlight that an improvement in efficiency by tuning the energy levels of the polymers by means of molecular design can be expected only if their truly optimized morphologies with fullerene in BHJ systems are materialized.

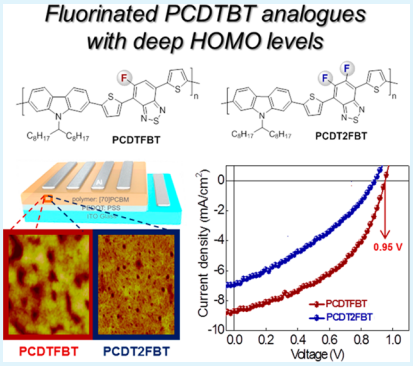

KEYWORDS: *bulk-heterojunction (BHJ) solar cells, 2,7-carbazole, PCDTBT, fluorination, low bandgap polymers, organic photovoltaics*

1. INTRODUCTION

Rapid and drastic advances in the performance of polymer-based bulk-heterojunction (BHJ) solar cells brighten the vision of organic photovoltaics for flexible, light-weight, and ultralow-cost electronic devices by inkjet printing and roll-to-roll processes.[1−7] It is well-known that the intrinsic properties of semiconducting polymers play determining roles in the overall performances of polymer BHJ solar cells. Thereby, research activities on new materials development have been almost exclusively focused on creating low bandgap polymers via donor (D)−acceptor (A) approach, so as to harvest more sunlight, which leads to higher short-circuit current density (J_{SC}).[3,8−14] However, a major drawback in lowering the bandgap of polymers is the moderate open-circuit voltage (V_{OC}), caused by their shallow highest occupied molecular orbital (HOMO) energy levels.

In this regard, poly(2,7-carbazole-*alt*-dithienylbenzothiadiazole) (PCDTBT, see Figure 1) is a superior example for a deep HOMO (−5.50 eV) as required by the "ideal" π-conjugated polymers, which is a crucial prerequisite to achieve a high V_{OC} and outstanding stability against oxidation.[12,15−18] Nevertheless, as reported, the inherent disadvantages of PCDTBT, such as slightly limited absorption range and relatively low carrier mobility led to the mediocre J_{SC}.[12,15−18]

In attempts to further optimize its light-harvesting and charge-transporting ability, we recently reported various PCDTBT-based structural derivatives, such as ladder-type PCDTBT[19] and naphthothiadiazole and selenophene analogues

Received: February 11, 2014
Accepted: April 18, 2014
Published: April 18, 2014

   dx.doi.org/10.1021/am500891z | ACS Appl. Mater. Interfaces 2014, 6, 7523−7534

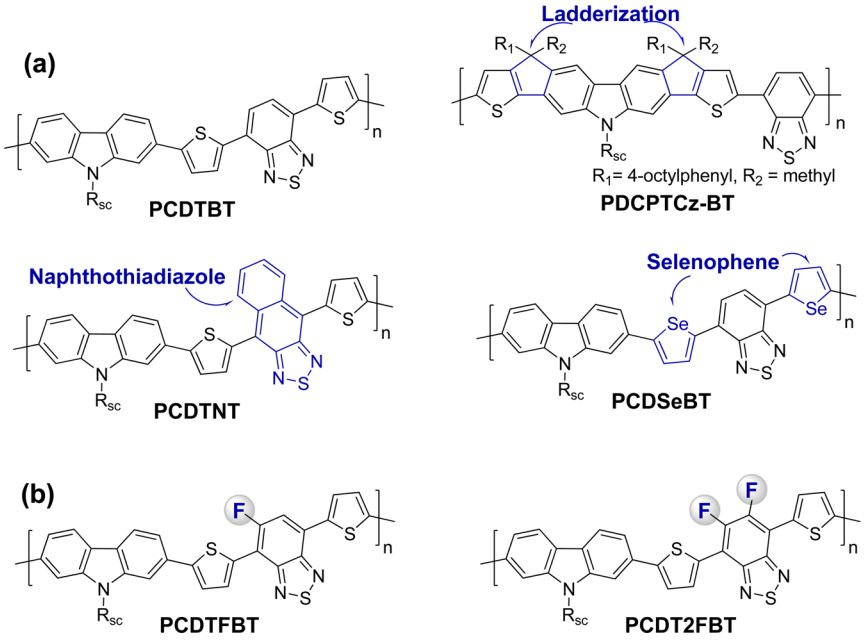

Figure 1. Chemical structures of (a) PCDTBT-based polymeric semiconductors studied by our research group and PCDTBT shown on the top/left and (b) novel fluorinated analogues of PCDTBT (**PCDTFBT** and **PCDT2FBT**) in the present study. R_{sc} = solubilizing alkyl chain.

Scheme 1. Synthetic Routes of PCDTFBT and PCDT2FBT[a]

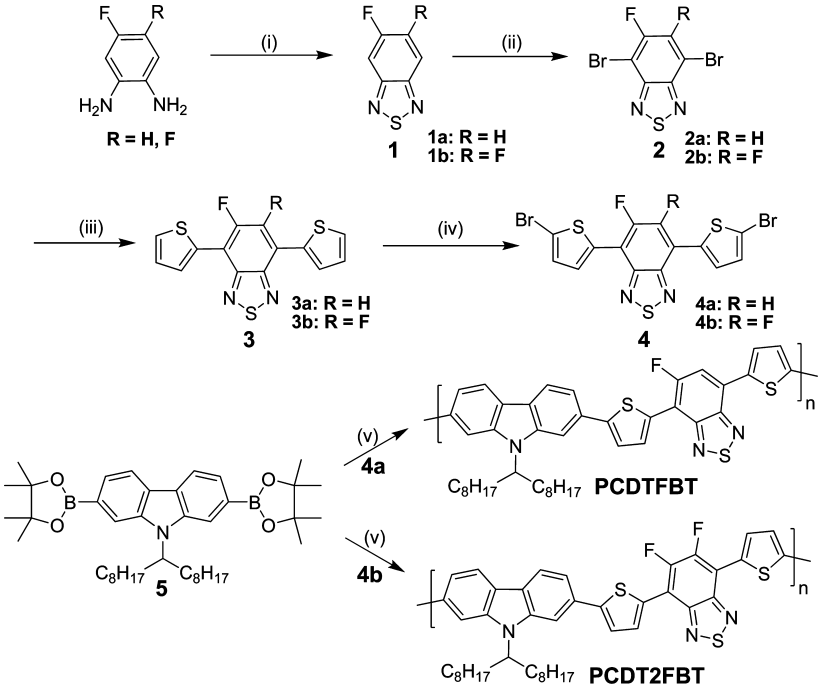

[a]Reagents and reaction conditions: (i) DCM, Et_3N, $SOCl_2$, 0 °C, dropwise, reflux, 5 h, 75%; (ii) HBr, Br_2, reflux, 120 °C, 48 h, 67%; (iii) 2-tributylstannyl thiophene, toluene, $Pd(pph_3)_4$, microwave, 140 °C, 3 h, 78%; (iv) NBS, THF, RT, 12 h, 86%; (v) toluene, $Pd_2(dba)_3$, P(*o*-tolyl)$_3$, aqueous K_3PO_4, Aliquat 336, 72 h.

of PCDTBT,[20,21] respectively (the structures shown in Figure 1). However, even in the successful demonstration regarding the extended absorption with deep-lying HOMOs, the resulting polymers did not yield devices with correspondingly high performances. This is probably a result of macroscopic state of matter for the polymers (solubility, molecular weight, polydispersity, and purity) and the morphological problems for given polymer/fullerene systems.

Recently, the introduction of fluorine (F) atoms onto conjugated polymer backbone has been proven to be an effective way to enhance the efficiency of BHJ solar cells.[22−34] The cause for this observation generally accounts for the lowering of the polymer HOMO energy level as well as the possible formation of the secondary bonding (e.g. C−F···H, F···S, and C−F···π_F) through inter- or intramolecular interactions. However, the actual dominating factors in the efficiency

dx.doi.org/10.1021/am500891z | ACS Appl. Mater. Interfaces 2014, 6, 7523−7534

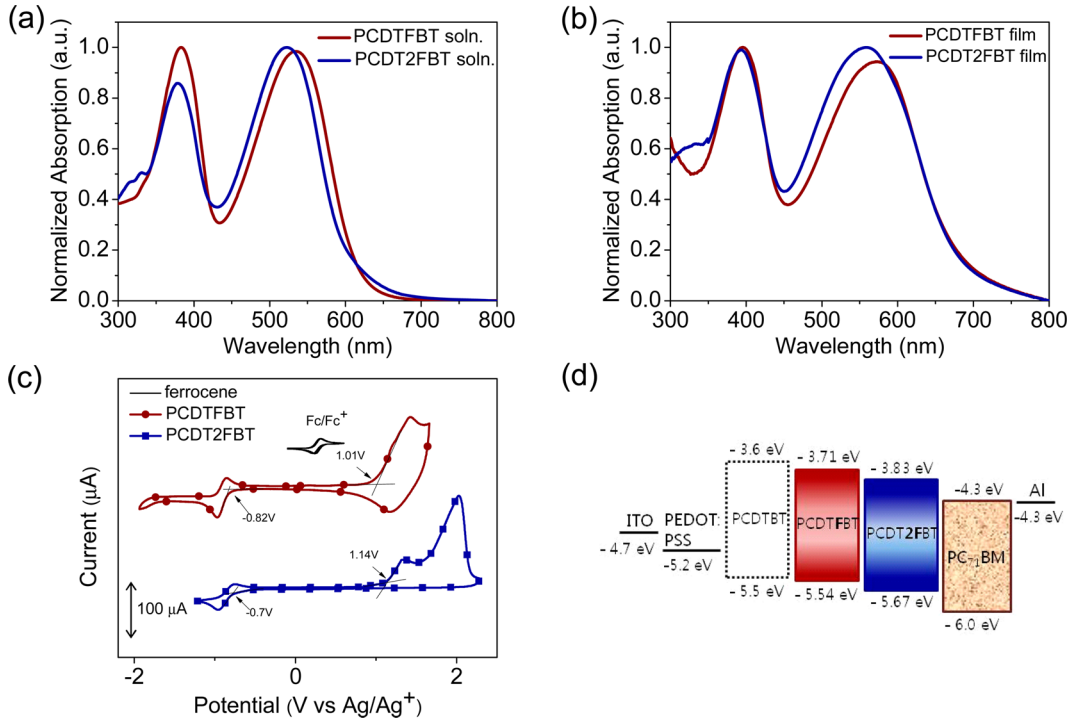

Figure 2. (a) Solutions and (b) thin films absorbance spectra of **PCDTFBT** and **PCDT2FBT**, (c) cyclic voltammogramms of the fluorinated polymer thin films on Pt electrodes in 0.1 M Bu_4NPF_6/CH_3CN at a scan rate of 50 mV s^{-1}, and (d) energy level diagrams of **PCDTFBT** and **PCDT2FBT** relative to the reported PCDTBT in the solution-processed conventional BHJ devices.

enhancement are not very clear and vary, depending on the systems.[22−25,29,30,32−36]

In this research, as another challenge for finding the success of molecular modification to PCDTBT backbone, we have firstly synthesized a series of its fluorinated analogues (**PCDTFBT** and **PCDT2FBT**) as shown in Figure 1, not only to investigate the effects of fluorination on the properties of PCDTBT but also to further uncover the underlying working principles of F atoms on each of the three photovoltaic parameters (V_{OC}, J_{SC}, and fill factor (FF)).

2. RESULTS AND DISCUSSION

2.1. Synthesis and Characterization. Scheme 1 shows the synthetic routes to prepare the intermediates and fluorinated target polymers. From mono- and difluoro-phenylenediamine as starting materials, **1a** and **1b** were prepared by an intramolecular cyclization with thionyl chloride in triethylamine, respectively.[37] Then, the corresponding dibromo compounds **2a** and **2b** were obtained by using bromine and hydrobromic acid. Under microwave-assisted condition, Pd-catalyzed Stille-type coupling reaction either of **2a** or **2b** and 2-tributylstannylthiophene gave **3a** or **3b**. Then, the addition of *N*-bromosuccinimide (NBS) to either of **3a** or **3b** in chloroform finished the synthesis of the dithienyl-fluorinated benzothiadiazole monomers (**4a** and **4b**).[38]

On the other hand, the diboronic ester co-monomer **5** based on 2,7-carbazole was synthesized according to the reported procedures.[18] Suzuki coupling polymerization using either of **4a** or **4b** and **5** in the presence of $Pd_2(dba)_3/P(o\text{-tolyl})_3$ as catalyst/ligand produced the corresponding polymers (**PCDTFBT** (1F) and **PCDT2FBT** (2F) are used to abbreviate mono-and di-fluorinated versions, respectively). Details of synthesis of monomers, polymerization, and their characterizations are given in the Experimental Sections.

Both the polymers were purified by successive Soxhlet extractions with methanol, acetone, hexane, and chloroform. Gel-permeation chromatography (GPC) analysis against polystyrene standard exhibited exhibits a number-averaged molecular mass (M_n) of 11.0×10^3 and 31.5×10^3 g mol^{-1} and polydispersity indices (PDIs) of 1.39 and 2.05 for **PCDTFBT** and **PCDT2FBT**, respectively. In addition, the polymers were structurally characterized by a combination of ^1H and ^{19}F NMR spectra (see Supporting Information Figure S9−S12).

Thermogravimetric analysis (TGA) shows that the onset decomposition temperatures (T_d) with 5 % weight loss of **PCDTFBT** and **PCDT2FBT** are around 450 and 437 °C, respectively (see Supporting Information Figure S13), indicating good thermal stability under nitrogen atmosphere. This implies that devices fabricated with the fluorinated polymers would be as much as stable as those of PCDTBT that are both stable in air at room temperature and capable of withstanding high temperatures for extended periods of time.[17,18]

2.2. Optical and Electrochemical Properties. Figure 2a and b show the UV−vis absorption spectra of **PCDTFBT** and **PCDT2FBT** in chlorobenzene (CB) solution and as thin films, respectively. Both the polymers exhibit two distinct absorption bands; a one at the high-energy region (270−400 nm), originating from the localized $\pi-\pi^*$ transition and a relatively broader one at the low-energy region (420−610 nm) induced by a typical intramolecular charge-transfer (ICT), as typically observed in D-A polymers including nonfluorinated analogous PCDTBT.[18]

Going from solution to the solid state, both the polymers have nearly identical features in their high-energy bands, while the low-energy bands are bathochromically shifted, implying the increased π-stacking form as well as electronic interactions in the solid state.[11,39] Notably, introducing more F atoms on the polymer backbone makes the maxima (λ_{max}) of the

dx.doi.org/10.1021/am500891z | ACS Appl. Mater. Interfaces 2014, 6, 7523−7534

polymers blue-shifted, that is, λ_{max} value of the **PCDT2FBT** film is 13 nm blue-shift from that of **PCDTFBT**. A similar effect was reported in fluorine-substituted oligomers and polymers.[29,31,34,40] The spectroscopic data of the polymers are summarized in Table 1, where the optical bandgap (E_g^{opt}) of

Table 1. Optical and Electrochemical Properties of the Polymers

polymer	λ_{max}^{soln} (nm)	λ_{max}^{film} (nm)	E_g^{opt} (eV)[a]	HOMO (eV)[b]	LUMO (eV)[b]	E_g^{elec} (eV)[c]
PCDTFBT	382, 535	395, 573	1.82	−5.54	−3.71	1.83
PCDT2FBT	378, 522	392, 560	1.82	−5.67	−3.83	1.84

[a]Calculated from the absorption band edge of the polymer films, $E_g^{opt} = 1240/\lambda_{edge}$. [b]Thin films were deposited on Pt electrodes with the solution of *n*-Bu_4NPF_6 in CH_3CN, versus Fc/Fc^+ at 50 mV s^{-1}. HOMO and LUMO were estimated from the onset oxidation and reduction potentials, respectively. [c]E_g^{elec} (eV) = |LUMO − HOMO| (eV).

the two polymers was determined from the onset of absorption (λ_{onset}). It is worth noting that despite the difference observed in λ_{max} values of the two polymers, the λ_{onset} values are almost unchanged, resulting in the same optical bands of 1.82 eV that is relatively lower than that of the nonfluorinated PCDTBT (1.88 eV). This can be partly attributed to a change in the polymer chain packing via the additional non-covalent interactions with a greater number of F atoms.

Figure 2c shows cyclic voltammogram (CV) of the polymer thin films in acetonitrile and the CV data are summarized in Table 1. The details for the measurements are given in Experimental Section. The CV curves of both **PCDTFBT** and **PCDT2FBT** cast films reveal quasi-reversible oxidation and reversible reduction behaviors. The HOMOs for **PCDTFBT** and **PCDT2FBT** are estimated to be −5.54 and −5.67 eV based on their onset redox potentials, respectively, and both are lower in energy than those of PCDTBT (−5.5 eV). These results are in agreement with the previous reports that fluorination leads to the lowering of the polymer HOMO level.[31,34,41] Thereby, both the polymers are expected to impart better air stability as well as a higher V_{OC} in BHJ solar cells than that of the PCDTBT-based devices.

When comparing singly versus doubly fluorinated polymers, accompanied by the further decrease on the HOMO observed by increasing the number of F atoms, **PCDT2FBT** yields LUMO energy levels at 0.12 eV lower than the **PCDTFBT** (−3.71 eV), resulting in a similar electrochemical bandgap (~1.83 eV). The estimated electrochemical bandgaps coincide well with the optical bandgaps measured for these polymers. In addition, the energy level positions of **PCDTFBT** and **PCDT2FBT** in BHJ solar cells together with those of PCDTBT are illustrated as shown in Figure 2d.

2.3. Computational Calculation. To understand the minimum-energy conformations and molecular orbital distributions by varying the number of F atoms, the optimized structures were computed by using density functional theory (DFT) calculation at B3LYP/6-31G level. The dioctyl alkyl chain on the model system was replaced by a methyl group for simplicity.

Among the three possible conformations of the structural dithienylbenzothiadiazole (DTBT) unit as positioning for the S atoms between the flanking thiophene and BT units (e.g., syn−syn, anti−anti, and syn−anti), the anti−anti conformers for both the DTFBT and DT2FBT, as shown in Figure 3a and b, show energetically stable molecular geometry with the lowest total energy in each single basic unit. Additionally, the dihedral angles between the BT core and the neighboring thiophene units are calculated to be less than 1°, contributing to the high molecular planarity for each polymer (see the top of Figure 3c and d). Figure 3c and d also show the molecular orbital distributions of HOMO and LUMO isosurfaces for each model dimer. HOMOs for both the models are well-delocalized over the whole conjugated backbone, while LUMOs are mainly distributed on the electron accepting BT blocks. We also observed the similar trends in the DFT calculation for the model trimers (see Figure S14−S16 in Supporting Information).

2.4. Organic Thin-Film Transistors (OTFTs) Characteristics. To test the charge-carrier transport capability of **PCDTFBT** and **PCDT2FBT**, typical bottom-gate/top-contact organic thin-film transistors (OTFTs) were fabricated by solution-processed spin-coating method. Figure 4 exhibits the output and transfer curves of the OTFTs tested with **PCDTFBT** and **PCDT2FBT**, showing typical *p*-type semi-

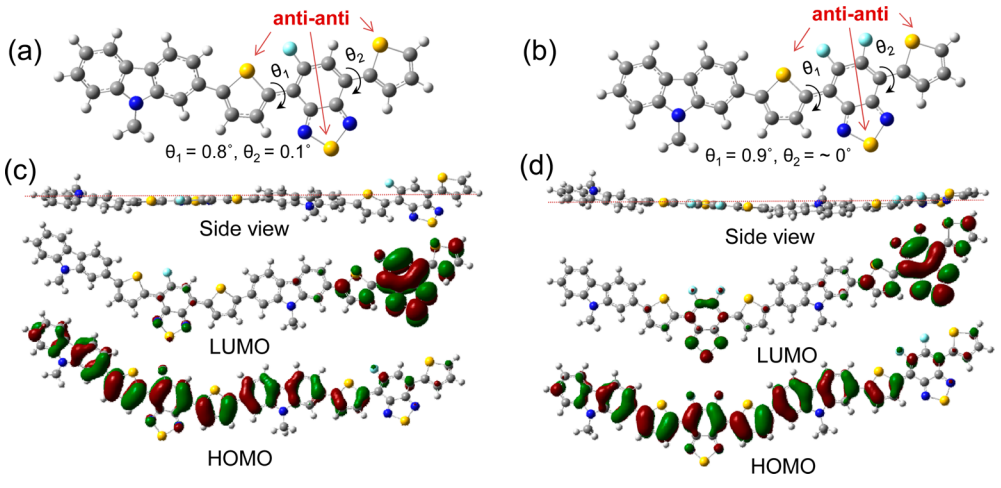

Figure 3. Optimized geometries with the lowest total energy of CDTFBT (a) and CDT2FBT (b). Side views and charge-density isosurfaces for the HOMO and LUMO levels of **PCDTFBT** (c) and **PCDT2FBT** (d) dimers (B3LYP/6-31G).

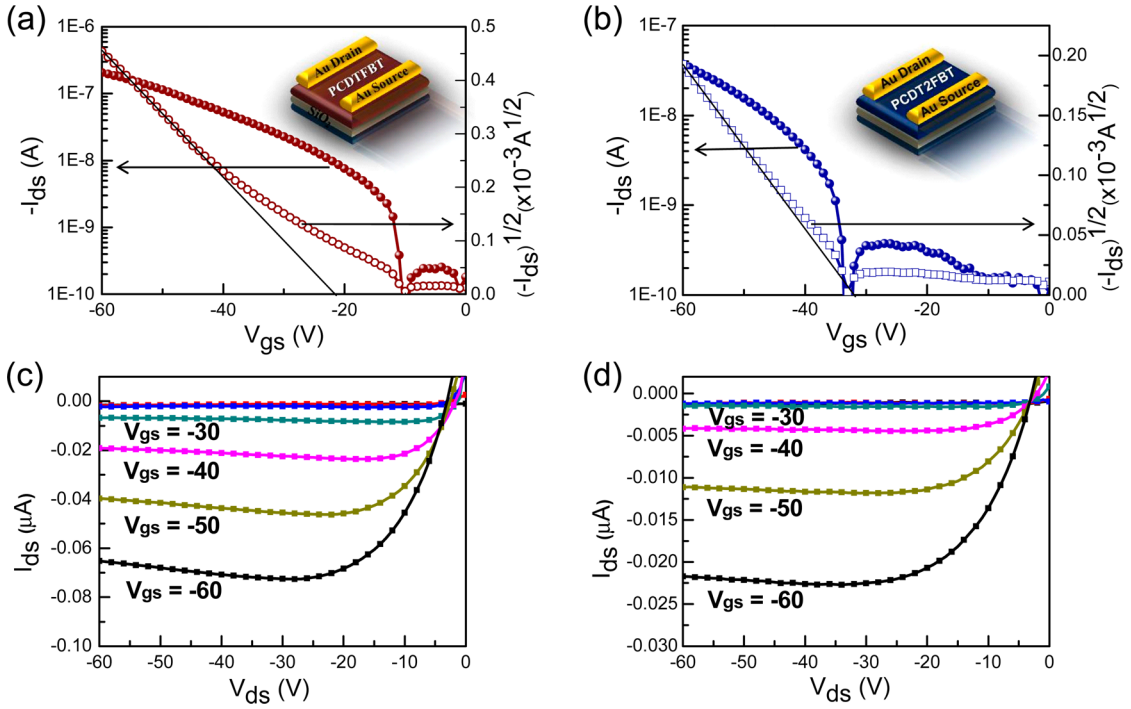

Figure 4. (a, b) Transfer curves in the saturated regime and (c, d) output characteristics for each OFET device (L = 50 μm, W = 2950 μm) based on **PCDTFBT** and **PCDT2FBT**, respectively. Insert: Schematic device configuration.

conductor behaviors. The hole mobilities were estimated from the slope of drain-to-source current $|I_{ds}|^{1/2}$ as a function of the gate voltage (V_{gs}) in the saturation regime. The **PCDTFBT** and **PCDT2FBT**-based OTFTs show the hole mobilities of 3.03 ($\pm$1.5) $\times$ 10^{-4} cm^2 V^{-1} s^{-1} and 9.50 ($\pm$2.6) $\times$ 10^{-5} cm^2 V^{-1} s^{-1}, threshold voltages (V_{Th}) of $-$20.85 and $-$30.28 V and on/off current ratios (I_{on}/I_{off}) of 8.60 $\times$ 10^2 and 2.25 $\times$ 10^2, respectively.

Since Yu and coworkers reported the effect of the net dipole moment on pseudocharge transfer characteristics in D$-$A polymers,[42,43] we also calculated for the ground to excited state dipole change for both fluorinated DTBTs and single repeat units of each polymer using time-dependent self consistent field (TD-SCF) method in the same basis set (see Figure S17 and Table S1 in Supporting Information), to propose a possible explanation for the superior OTFTs performance of **PCDTFBT**, as compared to **PCDT2FBT**. However, to certainly shed light on the validity of a correlation between the mobility and net dipole moment, perhaps more experimental evidence and detailed theoretical calculations in various polymers remain as the subject of future study.

2.5. Bulk-Heterojunction Solar Cell Performance. Photovoltaic effects of **PCDTFBT** and **PCDT2FBT** were investigated in BHJ solar cells with the conventional device configuration of glass/ITO/PEDOT:PSS/polymer:$PC_{71}BM$/Al. The blend ratios (w/w) of polymer and $PC_{71}BM$ were controlled from 1:1 to 1:4. To find a best condition, the photovoltaic properties were systematically screened in different solvents, concentrations, additives, and spin-coating speeds. Among such various conditions, the device performance was optimized when the blend was spin-coated with a ratio of 1:4 (w/w) by chlorobenzene (CB). The performances of both the polymers-based devices are considerably improved as a result of thermal annealing protocols. This is in contrast to PCDTBT:$PC_{71}BM$ system, in which thermal annealing reduced the photovoltaic parameters.[12,44]

Figure 5a shows current density-voltage ($J-V$) curves of photovoltaic devices based on **PCDTFBT** and **PCDT2FBT**, respectively under AM 1.5 G illumination from a calibrated solar simulator with irradiation intensity of 100 mW cm^{-2} and the parameters are listed in Table 2. In the pristine cells, the power conversion efficiencies (PCEs) of both the **PCDTFBT**- and **PCDT2FBT**-containing devices (PCE = 1.29$-$1.95 %) are limited by the unoptimized interpenetrating polymer/fullerene network. Upon optimization of the active layer morphology via the thermal annealing at 150 °C, **PCDTFBT**-based device exhibits the PCE of up to 3.96 %, with a J_{SC} of 9.04 mA cm^{-2}, a V_{OC} of 0.95 V, and a FF of 0.46. Although the performance of **PCDTFBT**-based device is somewhat lower than that from the reference cell based on PCDTBT:$PC_{71}BM$ for the sake of comparison (see Figure S18 and Table S2 in Supporting Information), the higher V_{OC} value (0.95 V) of **PCDTFBT** as compared with PCDTBT agrees with a lower-lying HOMO level. Furthermore, this V_{OC} value is nearly equaled the highest V_{OC} values for PCDTBT-based PSCs reported to date.[45$-$47] Note that, in stark contrast to PCDTBT:$PC_{71}BM$ system in which thermal annealing reduced the overall efficiency (see Figure S21 and Table S7 in Supporting Information), the performance of the fluorinated polymers-based devices for this study is considerably improved as a result of thermal treatment.

To further explore their devices performance, the effects of various solvent additives (1,8-diiodooctane (DIO), 1,4-butanedithiol (BDT), 1-chloronaphthalene (CN), 1,8-octanedithiol(ODT), diphenyl ether (DPE)) on the **PCDTFBT**:$PC_{71}BM$ (1:4 (w/w)), as well as polar solvent treatments (methanol and ethanol) were investigated (see Table S3$-$S4 in Supporting Information). In addition, considering the fact that for a given polymer structure, batch-to-batch variations in solubility, molecular weight, polydisper-

dx.doi.org/10.1021/am500891z | ACS Appl. Mater. Interfaces 2014, 6, 7523$-$7534

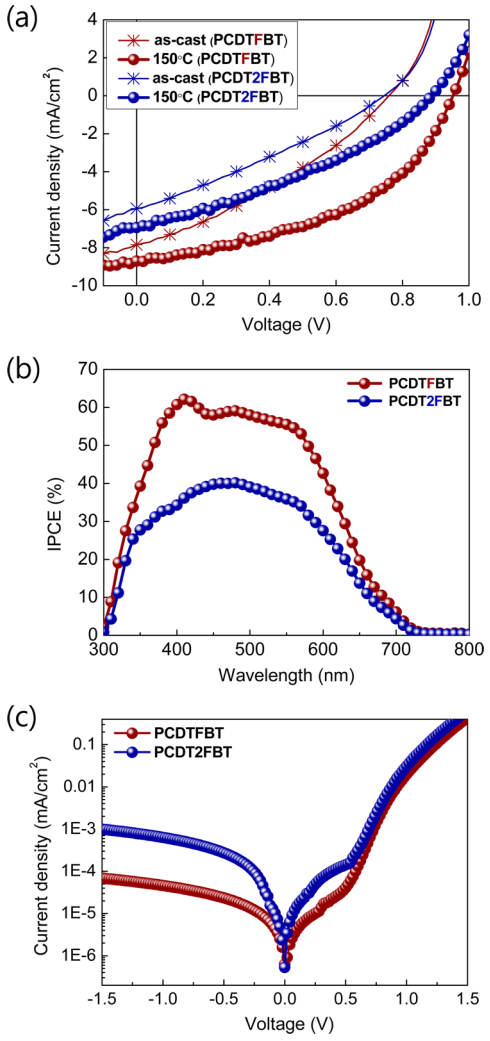

Figure 5. (a) Current density–voltage (J–V) characteristics and (b) incident photon-to-current efficiency (IPCE) of conventional devices with the blends of **PCDTFBT**:$PC_{71}BM$ and **PCDT2FBT**:$PC_{71}BM$ (1:4 w/w). (c) J–V characteristics in the dark for the blends of **PCDTFBT**:$PC_{71}BM$ and **PCDT2FBT**:$PC_{71}BM$ (1:4 w/w).

sity, and purity could lead to different processing properties and performance, we prepared various polymeric fractions through diverse strategies (e.g., Stille coupling, the utilization of microwave-assisted heating protocol, use of tiny amounts of catalyst, variation of solution concentrations, and replacement of $Pd_2(dba)_3$ with $Pd(PPh_3)_4$ as a catalyst, fractionation of the polymers by pre-GPC) (see Table S5 in Supporting Information). Interestingly, among the various attempts aforementioned, we find adding 2 % (v/v) DPE into the chlorobenzene solution of **PCDTFBT**:$PC_{71}BM$ prior to spin coating, the PCE dramatically increased up to 4.29 % (Figure 6, see Table S3–S5 for all other detailed photovoltaic performances in Supporting Information).

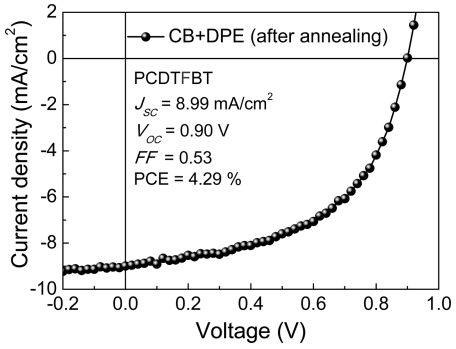

Figure 6. J–V characteristics of the device based on **PCDTFBT**:$PC_{71}BM$ blend with DPE (2% (v/v)) as an additive.

PCDTFBT in the inverted architecture (ITO/ZnO/polymer:$PC_{71}BM$/MoO_3/Au) employed in this study is inferior performance to that of the best typical solar cells above, because of the reduced J_{SC} and FF (see Figure S19, S20, and Table S6 in Supporting Information), however it delivers the same V_{OC} value (0.95 V). This is an expected result, considering the effect of F atoms as discussed in the Introduction. Naively, one may therefore expect the doubly-fluorinated **PCDT2FBT**-based device to have a further improved V_{OC} relative to that of **PCDTFBT**. However, the device based on **PCDT2FBT** is best PCE of only 2.07 %, accompanied by the moderate photovoltaic characteristics (J_{SC} = 6.94 $mAcm^{-2}$, a FF = 0.34, and even the decreased V_{OC} = 0.88 V).[25,27]

We measured the J–V curves in the dark to characterize the relation between the diode (reverse bias) saturation current density (J_0) and the V_{OC} using the devices based on **PCDTFBT**:$PC_{71}BM$ and **PCDT2FBT**:$PC_{71}BM$, respectively. The J_0, extracted from the intercept on the vertical axis from the logarithmic current curve with respect to voltage (Figure 5c), falls from around 10^{-3} to 10^{-4} $mAcm^{-2}$ with decreasing the number of fluorine atoms. Taking into account the following equation; $V_{OC} = n_{if}\, k_B T/q\, [\ln ((J_{SC} / J_0) + 1)]$, where J_0 is the dark saturation current density, k_B is the Boltzmann constant, T is the temperature, and n_{if} is the ideality factor.[48,49] The n_{if} was calculated to be 2.20 for the **PCDTFBT**:$PC_{71}BM$ device and 2.18 for the **PCDT2FBT**/$PC_{71}BM$ device, respectively, from the slope of J–V curves under dark condition in the space-charge-limited regime (see Figure S25 in Supporting Information) using the following equation: $n_{if} = [(k_B T/q) \times (\partial \ln J/\partial V)]^{-1}$.[50,51] Typical value of n_{if} is 2 (or less)[52] and the n_{if} of PCDTBT has been reported to be around 2.[53,54] **PCDTFBT**-based device shows the lower J_0 value, leading to the higher V_{OC} value than **PCDT2FBT**-based device.

Table 2. Summary of Solar Cell Characteristics of PCDTFBT and PCDT2FBT

active layer[a]	thickness (nm)	annealing temp (°C)[b]	J_{SC} (mA cm^{-2})	V_{OC} (V)	FF	PCE (%)[c]
PCDTFBT:$PC_{71}BM$	180	w/o	5.94	0.74	0.29	1.29 (1.16 ± 0.3)
		150	9.04	0.95	0.46	3.96 (3.68 ± 0.2)
PCDT2FBT:$PC_{71}BM$	146	w/o	7.84	0.76	0.33	1.95 (1.75 ± 0.1)
		150	6.94	0.88	0.34	2.07 (1.82 ± 0.3)

[a]polymer:$PC_{71}BM$ = 1:4 w/w. [b]10 min. [c]The photovoltaic parameters of the best performing devices are shown. The average values and standard deviations of the PCE based on more than 10 devices for each batch are also given in the parentheses.

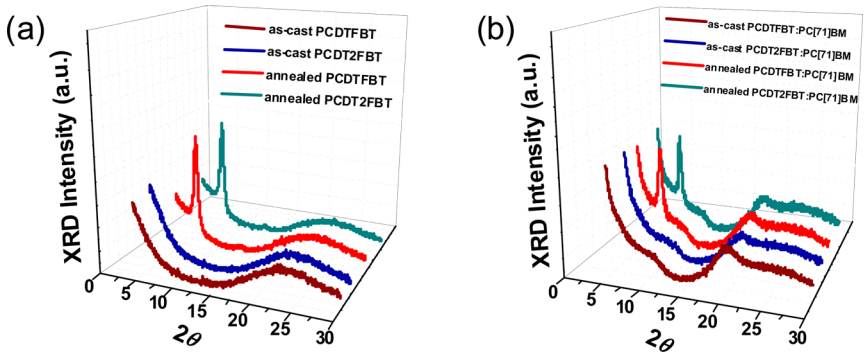

Figure 7. XRD patterns obtained from (a) pristine thin films of **PCDTFBT** and **PCDT2FBT** without and with thermal annealing and (b) blend films of **PCDTFBT**:$PC_{71}BM$ and **PCDT2FBT**:$PC_{71}BM$ (1:4 w/w) without and with thermal annealing at 150 °C on SiO_2/Si substrates.

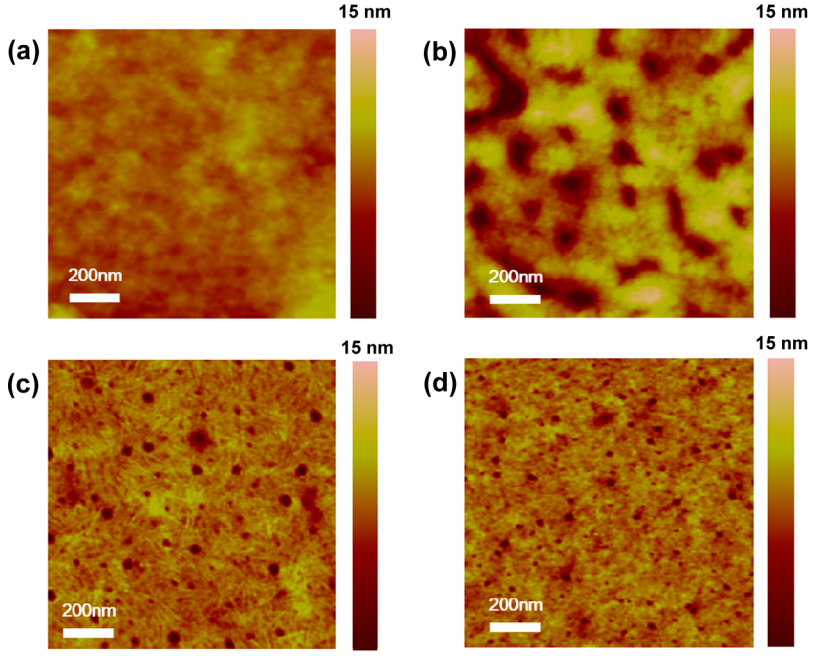

Figure 8. Surface morphology of blend films based on **PCDTFBT**:$PC_{71}BM$ (1:4 w/w) without (a) and with thermal annealing (b) and **PCDT2FBT**:$PC_{71}BM$ (1:4 w/w) without (c) and with thermal annealing (d).

The PCE with the limited V_{OC} of **PCDT2FBT**-based BHJ cells is still puzzling, however this suggests that other factors caused by inadequate morphology between D and A components beyond the contributor based solely on energy levels of HOMO and LUMO can be involved in the overall PCEs. A plausible explanation is that a formation of aggressive **PCDT2FBT** crystallinity via the sufficient driving force for C−F···H, and F···S, and C−F···π_F interactions as well as the fluorophobicity effect[29] for fullerene molecules is detrimental to the morphology quality in BHJ system, leading to a reduced shunt resistance[55,56] and increased bimolecular recombinations.[57−60]

To further verify the accuracy of the measurement, incident photon-to-current efficiency (IPCE) spectra were measured for the corresponding best devices. As depicted in Figure 5(b), both the polymers show IPCE contributions at wavelengths in the range from 300 to 700 nm. **PCDTFBT** shows relatively higher photoconversion efficiencies of ∼60 % than those of **PCDT2FBT** (∼40 %) throughout their absorption ranges. The integrated J_{SC} from IPCE data agrees well with the data from J−V curves. Almost quenched photoluminescence (PL) data for both polymer in polymer:$PC_{71}BM$ blends indicated that not only does the efficient photoinduced charge transfer occur, but also this loss of photocurrent cannot be assigned to exciton diffusion limitations (see Supporting Information Figure S26).

The hole and electron mobilities of the fluorinated polymer:$PC_{71}BM$ blend systems (1:4 (w/w)) were measured by the space-charge-limited current (SCLC) method, as shown in Supporting Information Figure S24 (see Supporting Information Table S10). The hole (μ_h) and electron mobilities (μ_e) for **PCDTFBT**:$PC_{71}BM$ blend were obtained to be 2.87×10^{-4} and 1.64×10^{-4} $cm^2\ V^{-1}\ s^{-1}$ with the thermal annealing, respectively, which are about an order of magnitude higher than those of **PCDT2FBT** blend ($\mu_h = 3.49 \times 10^{-5}$ and $\mu_e = 7.27 \times 10^{-5}$ $cm^2\ V^{-1}\ s^{-1}$). The charge-carrier mobilities such as higher and more balanced values can roughly track the trend in overall PCE of both the polymers.[20]

2.6. Thin-Film Morphology. To further determine the influence of the fluorine substitutions on the bulk morphology, X-ray diffraction (XRD) analysis was used to examine the thin films of each pure polymer and as-spun blends of polymer:$PC_{71}BM$, respectively (Figure 7). The XRD patterns

dx.doi.org/10.1021/am500891z | ACS Appl. Mater. Interfaces 2014, 6, 7523−7534

from the **PCDTFBT** and **PCDT2FBT**-only films at 22.68° and 23.33° respectively, show the $d(010)$ reflections, characteristic of the $\pi-\pi$ stacking of the polymer backbones,[61] while there are no observable (100) reflection. On the other hand, both the annealed films exhibit significant sharpening and intensification of the (100) reflections (2θ = 6.54° for **PCDTFBT** and 6.58° for **PCDT2FBT**), along with the presence of the slightly shifted *(010)* peaks. Notably, the observed π-stacking distances ($d(010)$ = 3.8−3.9 Å) of both the as-spun and annealed films of the polymers are shorter than that of the reported PCDTBT film ($d(010)^{PCDTBT}$ = 4.4 Å),[12] evidencing a closer molecular ordering of the fluorinated polymers. When $PC_{71}BM$ is blended with the polymers, it is clear that the molecular packing either along the side-chain or the π-stacking directions seems to be changed. The diffraction peaks caused by $PC_{71}BM$ crystallites were not detected from pure $PC_{71}BM$-only films in our control experiments (see Supporting Information Figure S27). This is in contrast with other works in which the sharp crystalline $PC_{71}BM$ peaks can be observed at ∼19.2°.[62,63] On the other hand, it is interesting to point out that we observe the new diffractions at 2θ = 19.0−19.3° ranges in all the blended films, leading to a significant broadening of the peaks appearing around 17−24°. A possible explanation for this is that the $PC_{71}BM$ molecules can diffuse through the polymer matrix and form large single crystals in the blend systems. In addition, the $d(100)$-spacing peaks for both the annealed blend films are somewhat shifted, which is expanded by ∼0.4 Å, compared to their corresponding their pristine polymer films. It is apparent that there is a co-existence of the (010) and (100) peaks for both the post-annealed polymers.

According to the XRD results, one can conclude that the thermal annealing leads to in a reorientation of the polymers both at the surface and in the interior of the films, enhancing a preference in the face-on orientations. This is probably of consequence for better photovoltaic device performance on the devices presented here via the use of the thermal annealing.

We also investigated the film morphology of the polymer blend films processed with and without thermal annealing by using atomic force microscopy (AFM). From the height images (Figure 8), the annealed surface processed **PCDTFBT** (rms = 2.54 nm) is rougher than that without annealing (rms =0.38 nm), attributed to a morphology of appropriate phase separation with fullerene aggregates as well as a interpenetrating D and A domains.[64] In the both before and after annealing cases of the **PCDT2FBT**-based film, the AFM reveals uniform and smooth surfaces (0.47−0.53 nm) and the interpenetrating networks are not difficult to be distinguished. The more favorable morphology of **PCDTFBT**:$PC_{71}BM$ blend films after the thermal annealing can mainly contribute to the high performance of this polymer, as compared to the **PCDT2FBT**-based devices. Note that PCDTBT film shows smaller rms values being almost unchanged upon the annealing process (0.18−0.26 nm) (see Supporting Information Figure S28).

3. CONCLUSION

In summary, the synthesis of two novel fluorinated analogues of PCDTBT, namely, **PCDTFBT** (1F) and **PCDT2FBT** (2F), designed by either singly- or doubly-fluorination of the BT unit on the repeat unit, have been described, aiming to render favorable properties for the lowering of the polymer HOMO energy levels as well as the creation of the secondary bonding toward further improving the photovoltaic parameters. Both experimental results and theoretical calculations have shown that the incorporation of F atoms to the polymer backbone can fine-tune the polymer energy levels, charge-carrier transport capability, and molecular packing. The resulting polymers show the desirable deeper HOMOs (−5.54 to −5.67 eV) and LUMOs (−3.71 to −3.83 eV) than its nonfluorinated PCDTBT (HOMO = −5.5 eV and LUMO = −3.6 eV), possibly allowing a high V_{OC} and J_{SC}. On the basis of the **PCDTFBT** systems, BHJ solar cells with a PCE as high as 3.96 % have been realized by noticeably increasing the V_{OC} of 0.95 V, which ties close to the hitherto reported highest V_{OC} values of PSCs based on PCDTBT derivatives. In the quest to further improve the PCEs, the **PCDTFBT**-based device processed with 2 % (v/v) DPE solvent additive exhibits an increase in the PCE of up to 4.29 %.

Regarding the relative deeper-lying HOMO level via the multi-fluorination, the device derived from **PCDT2FBT** is expected to show better performance with the further improved V_{OC} value. Nevertheless, the only moderate PCE of 2.07 % with even the somewhat decrease in V_{OC} (0.88 V) is observed. Therefore, the results shown in this study indicate that the successful application of F atoms to any conjugated polymer for BHJ solar cells can only be realized only with a truly optimized morphology that varies from one polymer/fullerene system to the other. Though investigations to further understand the impact of the F atoms on the morphology, self-assembly behavior, and exciton-related dynamics are currently underway, it is still believed that the triumph morphology remains on the top of research priorities for highly efficient BHJ systems.

4. EXPERIMENTAL SECTION

4.1. Synthesis of 5-Fluoro-2,1,3-benzothiadiazole (1a). 4-Fluoro-1,2-phenylamine (5 g, 39.6 mmol) was dissolved in 50 ml of dry dichloromethane (DCM). Then, triethylamine (23 mL, 163 mmol) was added. The reaction mixture was cooled to 0 °C. Thionyl chloride ($SOCl_2$) (6.0 ml, 82 mmol) was added dropwise. Then, reaction mixture was allowed to reflux for 5 h. After it was cooled to room temperature, the mixture was poured into ice-water and extracted with DCM. The organic layer was dried with $MgSO_4$ and the solvent was evaporated in vacuo. The product was purified by column chromatography on silica gel using hexane/DCM (10/2) as eluent. The isolated yield = 75 %. ^{1}H NMR (600 MHz, $CDCl_3$): δ (ppm) 7.98 (dd, 1H, J = 9.6, 5.4 Hz), 7.60 (dd, 1H, J = 9, 3 Hz), 7.43 (td, 1H, J = 9, 2.4 Hz) (Supporting Information Figure S1. ^{13}C NMR (150 MHz, $CDCl_3$): δ (ppm) 164.33, 162.65, 154.93, 151.98, 122.53, 121.40, 104.85, 104.69. Anal. Calcd for $C_6H_3FN_2S$: C, 46.74; H, 1.96; F, 12.32; N, 18.17; S, 20.80. Found: C, 46.53; H, 1.92; N, 17.92; S, 21.08.

4.2. Synthesis of 5,6-Difluoro-2,1,3-benzothiadiazole (1b). **1b** was synthesized by following similar procedure to **1a**; the isolated yield = 62 %. ^{1}H NMR (600 MHz, $CDCl_3$): δ (ppm) 7.74 (t, 2H, J = 9.0 Hz) (Supporting Information Figure S2). ^{13}C NMR (150 MHz, $CDCl_3$): δ (ppm) 154.67, 154.53, 153.07, 152.81, 150.78, 106.15, 105.04.105.01. Anal. Calcd for $C_6H_2F_2N_2S$: C, 41.86; H, 1.17; F, 22.07; N, 16.27; S, 18.63. Found: C, 42.03; H, 1.09; N, 15.99; S, 18.47.

4.3. Synthesis of 4,7-Dibromo-5-fluoro-2,1,3-benzothiadiazole (2a). **1a** (1.84 g, 11.9 mmol) and HBr (30 mL) were taken in a round bottom flask. 5.5 mL of bromine was added slowly. The reaction mixture was refluxed at 120 °C for 2 days. Then, it was cooled down to room temperature. The excess of bromine was quenched with saturated $NaHSO_3$ solution. The precipitate formed was filtered off and washed several times with water. The product was recrystallized two times from ethanol (the isolated yield = 67 %). ^{1}H NMR (600 MHz, $CDCl_3$): δ (ppm) 7.78 (d, 1H, J = 7.8 Hz) (Supporting Information Figure S3). ^{13}C NMR (150 MHz, $CDCl_3$): δ (ppm) 160.91, 159.22, 152.73, 150.26, 123.93, 113.99, 98.25. Anal. Calcd for $C_6HBr_2FN_2S$: C, 23.10; H, 0.32; Br, 51.23; F, 6.09; N, 8.98; S, 10.28.

Found: C, 22.95; H, 0.29; N, 8.8; S, 10.05. MS (EI) Calcd: 311.8. Found: 312.

4.4. Synthesis of 4,7-Dibromo-5,6-fluoro-2,1,3-benzothiadiazole (2b). **2b** was synthesized by following similar procedure to **2a**; the isolated yield = 66 %. (Supporting Information Figure S4). ^{13}C NMR (150 MHz, $CDCl_3$): δ (ppm) 152.69, 152.55, 150.96, 150.82, 148.81, 148.79, 148.78, 99.40, 99.35, 99.29, 99.24. Anal. Calcd for $C_6Br_2F_2N_2S$: C, 21.84; Br, 48.43; F, 11.52; N, 8.49; S, 9.72. Found: C, 21.60; N, 8.26; S, 9.53. MS (EI) Calcd: 329.8. Found: 330.

4.5. Synthesis of 4,7-Di(2′-thiophenyl)-5-fluoro-2,1,3-benzothiadiazole (3a). **2a** (1 g, 3.2 mmol), trimethyl(thiophen-2-yl)stannane (2.69 g, 7.2 mmol), $Pd(PPh_3)_4$ (0.150 g, 0.129 mmol) were taken in a 30 mL microwave vial. Anhydrous toluene (20 mL) was injected. The mixture was then purged with nitrogen gas for 10 min. The vial was then sealed with a snap cap and subjected to the following reaction conditions in a microwave reactor (Anton Paar Monowave 300, 140 °C for 3 h). The reaction mixture was then cooled to room temperature. The solvent was evaporated and the product was purified by column chromatography (silica gel) using dichloromethane/hexane = 1:10 as the eluent (the isolated yield = 78 %).^{1}H NMR (600 MHz, $CDCl_3$): δ (ppm) 8.26 (d, 1H, J = 3.6 Hz), 8.12 (d, 1H, J = 3.6 Hz), 7.77 (d, 1H, J = 13.2 Hz), 7.56 (d, 1H, J = 4.8 Hz), 7.50 (d, 1H, J = 5.5 Hz), 7.24 (t, 1H, J = 4.2 Hz), 7.21 (t, 1H, J = 4.2 Hz) (Supporting Information Figure S5). ^{13}C NMR (150 MHz, $CDCl_3$): δ (ppm) 159.71, 158.02, 153.50, 149.76, 137.95, 132.44, 130.12, 128.39, 128.12, 127.93, 127.22, 125.97, 117.10, 111.27. Anal. Calcd. for $C_{14}H_7FN_2S_3$: C, 52.81; H, 2.22; F, 5.97; N, 8.80; S, 30.21. Found: C, 52.66; H, 2.17; N, 8.54; S, 29.95. MS (EI) Calcd: 317.9. Found: 318.

4.6. Synthesis of 4,7-Di(2′-thiophenyl)-5,6-fluoro-2,1,3-benzothiadiazole (3b). **3b** was synthesized by following similar procedure to **3a**; the isolated yield = 84 %. ^{1}H NMR (600 MHz, $CDCl_3$): δ (ppm) 8.30 (d, 2H, J = 3.3 Hz), 7.62 (dd, 2H, J = 5.1, 0.9 Hz), 7.27 (t, 2H, J = 4.5 Hz) (Supporting Information Figure S6). Anal. Calcd for $C_{14}H_6F_2N_2S_3$: C, 49.98; H, 1.80; F, 11.30; N, 8.33; S, 28.60. Found: C, 49.69; H, 1.77; N, 8.12; S, 28.34. MS (EI) Calcd: 335.9. Found: 336.

4.7. Synthesis of 4,7-Bis(5′-bromo-2′-thiophenyl)-5-fluoro-2,1,3-benzothiadiazole (4a). **3a** (0.3 g, 0.94 mmol) was dissolved in 40 mL of THF. *N*-bromosuccinimide (NBS) (0.402 g, 2.2 mmol) was added to the solution portion wise. The reaction mixture was stirred at room temperature for 12 h and water was added. Then the red-orange solid was filtered and washed several times with water and ethanol, and then dried under vacuum (the isolated yield = 86 %). ^{1}H NMR (600 MHz, $CDCl_3$): δ (ppm) 8.01 (d, 1H, J = 4.2 Hz), 7.80 (d, 1H, J = 4.2 Hz), 7.69 (d, 1H, J = 12.6 Hz), 7.18 (d, 1H, J = 3.6 Hz), 7.17 (d, 1H, J = 4.2 Hz) (Supporting Information Figure S7). Anal. Calcd for $C_{14}H_5Br_2FN_2S_3$: C, 35.31; H, 1.06; Br, 33.56; F, 3.99; N, 5.88; S, 20.20. Found: C, 35.66; H, 1.06; N, 5.7; S, 20.04. MS (EI) Calcd: 475.8. Found: 476.

4.8. Synthesis of 4,7-Bis(5′-bromo-2′-thiophenyl)-5,6-fluoro-2,1,3-benzothiadiazole (4b). **4b** was synthesized by following similar procedure to **3b**; the isolated yield = 80 %. ^{1}H NMR (600 MHz, $CDCl_3$): δ (ppm) 8.04 (d, 2H, J = 4.2 Hz), 7.22 (d, 2H, J = 4.2 Hz) (Supporting Information Figure S8). Anal. Calcd. for $C_{14}H_4Br_2F_2N_2S_3$: C, 34.03; H, 0.82; Br, 32.34; F, 7.69; N, 5.67; S, 19.46. Found: C, 34.10; H, 0.79; N, 5.72; S, 19.19. MS (EI) Calcd: 493.8. Found: 494.

4.9. Synthesis of Poly[*N*-9″-heptadecanyl-2,7-carbazole-*alt*-5,5-(4,7-di-2′-thienyl-5-fluoro-2,1,3-benzothiadiazole)] (PCDTFBT). **4a** (145 mg, 0.30 mmol) and **5** (200 mg, 0.30 mmol) were dissolved in anhydrous toluene (10 mL) and argon-bubbled for 10 min in a tube-type schlenk flask. $Pd_2(dba)_3$ (4.2 mg, 3 mol %, 4.5 μmol), P(o-tolyl)$_3$ (8.2 mg, 27 μmol), K_3PO_4 (254 mg, 1.2 mmol), distilled water (3 ml), and Aliquat 336 (1 drop) were sequentially added into the flask. The reaction mixture was stirred and refluxed for 48 h before end-capping with phenylboronic acid and bromobenzene (0.03 mmol each). After it was cooled down, the mixture was poured into MeOH. The precipitate was collected and then purified by Soxhlet extraction with acetone, methanol, hexane, and chloroform in sequence. The chloroform fraction was concentrated to small volume, which was followed by re-precipitation in MeOH. Finally, the precipitate was collected by suction filtration and completely dried in vacuum oven to afford deep purple polymer powder (120 mg, 55 %). GPC analysis, M_n = 11 000 g mol^{-1}, M_w = 15,290 g mol^{-1}, and PDI = 1.39 (against PS standard). ^{1}H NMR (600 MHz, $CDCl_2CDCl_2$, 300 K): δ (ppm) 8.34 (br, 1H), 8.21 (br, 1H), 8.12 (br, 2H), 7.84 (br, 2H), 7.73 (br, 1H), 7.56 (br, 4H), 4.69 (br, 1H), 2.40 (br, 2H), 2.08 (br, 2H), 1.30−1.16 (br, 24H), 0.88−0.80 (br, 6H) (Supporting Information Figure S9). ^{19}F NMR (564 MHz, $CDCl_3$): δ (ppm) −108.20.

4.10. Synthesis of Poly[*N*-9″-heptadecanyl-2,7-carbazole-*alt*-5,5-(4,7-di-2′-thienyl-5,6-fluoro-2,1,3-benzothiadiazole)] (PCDT2FBT). Synthesis of Poly[*N*-9″-heptadecanyl-2,7-carbazole-*alt*-5,5-(4,7-di-2′-thienyl-5,6-fluoro-2,1,3-benzothiadiazole)] (**PCDT2FBT**) was carried out in the same manner as **PCDTFBT**. **4b** (150 mg, 0.30 mmol), **5** (200 mg, 0.30 mmol), anhydrous toluene (10 ml), $Pd_2(dba)_3$ (4.2 mg, 3 mol %, 4.5 μmol), P(o-tolyl)$_3$ (8.2 mg, 27 μmol), K_3PO_4 (254 mg, 1.2 mmol), distilled water (3 mL), and Aliquat 336 (1 drop). **PCDT2FBT** (100 mg, 44 %). GPC analysis, M_n = 31 500 g mol^{-1}, M_w = 64,500 g mol^{-1}, and PDI = 2.05 (against PS standard). ^{1}H NMR (600 MHz, $CDCl_2CDCl_2$, 300 K): δ (ppm) 8.35 (br, 1H), 8.06 (br, 1H), 7.89 (br, 1H), 7.70 (br, 1H), 7.55 (br, 4H), 7.22 (br, 2H), 4.64 (br, 1H), 2.38 (br, 2H), 2.04 (br, 2H), 1.33−1.17 (br, 24H), 0.90−0.81 (br, 6H) (Supporting Information Figure S10). ^{19}F NMR (564 MHz, $CDCl_3$): δ (ppm) −128.12.

4.11. Materials and General Characterization Methods. All chemicals and solvents were purchased from Aldrich and Acros chemical companies and used as received without further purification. THF was distilled over sodium/benzophenone. 4-Fluoro-1,2-phenyldiamine and 4,5-difluoro-1,2-phenyldiamine were purchased from Alfa Aesar and TCI chemical incorporation, respectively. 2,7-bis(4′,4′,5′,5′-tetramethyl-1′,3′,2′-dioxaborolan-2′-yl)-*N*-9″-heptadecanylcarbazole (**5**) was prepared according to reported procedures.[18] ^{1}H, ^{13}C, and ^{19}F NMR were recorded on Varian VNRS 600 MHz spectrophotometer using the deuterated chloroform ($CDCl_3$) or tetrachloroethane ($CDCl_2CDCl_2$) with TMS as an internal standard. Elemental analyses of carbon, hydrogen and sulfur were carried out with Flesh 2000 elemental analyzer and mass spectra were measured with a Varian 450-GC and 320-MS. Thermogravimetric analysis (TGA) was performed using Q200 from TA Instruments on heating rate of 10 °C min^{-1} in N_2 atmosphere. To investigate molecular weight and polydispersity index (PDI) of the new polymers, gel permeation chromatography (GPC) was carried out with Agilent 1200 series and miniDAWN TREOS using THF as solvent against PS as a standard. UV−vis absorption spectra were recorded on a Varian Carry 5000 spectrophotometer at room temperature. Photoluminescence was measured by Cary Eclipse. The electrochemical data was obtained from VersaSTAT3 Princeton Applied Research Potentiostat in a three-electrode cell system using 0.1 M tetrabutylammonium hexafluorophosphate (Bu_4NPF_6) in acetonitrile as the electrolyte at a scan rate of 50 mV/s at room temperature. Ag/Ag^+ 0.1 M of $AgNO_3$ in acetonitrile) as a reference electrode, a platinum counter electrode, and a polymer-coated platinum working electrode were used, respectively. The Ag/Ag^+ reference electrode was calibrated using a ferrocene/ferrocenium redox couple as an external standard, whose oxidation potential is set at −4.8 eV with respect to zero vacuum level. The HOMO energy levels were obtained from the equation HOMO (eV) = $-(E_{(ox)}{}^{onset} - E_{(ferrocene)}{}^{onset} + 4.8)$. The LUMO levels of polymers were obtained from the equation LUMO (eV) = $-(E_{(red)}{}^{onset} - E_{(ferrocene)}{}^{onset} + 4.8)$. AFM measurements were performed using a Digital Instruments dimension atomic force microscope controlled by a Nanoscope scanning probe microscope controller. XRD analysis for all of the films was performed with a Bruker D8 Advance high resolution X-ray diffractometer. The thin films cast from solution (onto a Si wafer as substrate) was studied by X-ray diffraction (XRD) analysis. The radiation was a monochromatized Cu Kα beam with wavelength λ = 0.15418 nm.

4.12. Fabrication of Field-Effect Transistors. Highly doped n^+-Si wafers were used as substrates and a layer of 200 nm of silicon

dioxide (SiO_2 grown by thermal oxidation) was used as the gate dielectric layer. Au (60 nm) was successively evaporated with shadow mask to obtain source and drain electrodes. The interdigitated structure of the source−drain contacts determined a channel length of 50 μm and a channel width of 2950 μm. Substrates were cleaned by acetone, isopropanol and dried at 100 °C oven for 20 min, and treated with octadecyltrichlorosilane (OTS) at room temperature for over 12 h to treat the surface. Organic semiconductor layers (60 nm) were deposited by spin-coating at 2000 rpm. All fabrication processes were carried out in a glove box filled with N_2. Electrical characterization was performed using a Keithley semiconductor parametric analyzer (Keithley 4200-SCS) under N_2 atmosphere. The electron mobility (μ) was determined using the following equation in the saturation regime; $I_{ds} = (WC_i/2L) \times \mu \times (V_{gs}-V_T)^2$, where C_i is the capacitance per unit area of the SiO_2 dielectric (C_i = 15 nF/cm^2) and V_T is the threshold voltage.

4.13. Fabrication of bulk heterojunction solar cells. Polymer solar cell devices were fabricated according to the following procedure. First, the ITO-coated glass substrate was cleaned with detergent, then ultrasonicated in distilled water, acetone and isopropyl alcohol, and then dried overnight in an oven at 100 °C. Poly(3,4-ethylenedioxythiophene):poly(styrenesulfonate) (PEDOT:PSS) was spin-cast at 4000 rpm for 40 s. The substrate was then dried for 10 min at 140 °C in air. Subsequently, it was moved into a glove box for spin-coating the active layer. The mixed solution of **PCDTFBT**:$PC_{71}BM$ (from 1:1 to 1:4 (w/w)), **PCDT2FBT**:$PC_{71}BM$ (from 1:1 to 1:4 (w/w)) and **PCDTBT**:$PC_{71}BM$ (from 1:1 to 1:4 (w/w)) in chlorobenzene (CB) were then spin-coated at 1500 rpm for 60 s on top of the PEDOT:PSS layer to obtain a BHJ film, respectively. Those samples were brought into a vacuum system (~10^{-7} Torr), and an Al electrode (100 nm) was deposited on top of the each BHJ layer. Typical devices were thermally annealed for 10 min at 120, 140, and 150 °C, gradually. In addition, the device structures of the hole and electron only devices are ITO/PEDOT:PSS/(**PCDTFBT** or **PCDT2FBT**):$PC_{71}BM$/Au and FTO/(**PCDTFBT** or **PCDT2FBT**):$PC_{71}BM$/Al, respectively. Typical devices were thermally annealed. The samples were not exposed to ambient air after being loaded into the glove box. The solar cell devices were illuminated at an intensity of 100 mW cm^{-2}. For more accurate information, the IPCE measurements were carried out with QEX7. The space-charge-limited current (SCLC) mobilities were estimated the Mott−Gurney square law $J_{SCLC} = 9/8 \times \varepsilon_r\varepsilon_0 \times \mu(V^2/L^3)$, where ε_r is the dielectric constant of the material, ε_0 is the permittivity of free space, L is the distance between the cathode and anode, which is equivalent to the film thickness, and V is the applied voltage.

■ ASSOCIATED CONTENT

Ⓢ Supporting Information

^{1}H NMR, ^{19}F NMR, and TGA data for polymers, additional DFT calculation results for trimmers, and inverted solar cell performances. This material is available free of charge via the Internet at http://pubs.acs.org.

■ AUTHOR INFORMATION

Corresponding Authors

*E-mail: jykim@unist.ac.kr.

*E-mail: yang@unist.ac.kr. Tel:+82-52-217-2920.

Author Contributions

J.K. and M.H.Y. contributed equally to this paper.

Notes

The authors declare no competing financial interest.

■ ACKNOWLEDGMENTS

This research was supported by Basic Science Research Program through the National Research Foundation of Korea (NRF) funded by the Ministry of Science, ICT and Future Planning (Grant No. 2013R1A1A1A05004475, 2010-0019408, NRF-2009-C1AAA001-0093020), BK21 Plus Program (META-material-based Energy Harvest and Storage Technologies, 10Z20130011057), New & Renewable Energy of the Korea Institute of Energy Technology Evaluation and Planning (KETEP) grant funded by the Korea government Ministry of Knowledge Economy (No. 20123010010140), and the International Cooperation of the Korea Institute of Energy Technology Evaluation and Planning (KETEP) grant funded by the Korea government Ministry of Knowledge Economy (2012T100100740). This work is also supported by Development Program of the Korea Institute of Energy Research (KIER) (B4-2424).

■ REFERENCES

(1) Yu, G.; Gao, J.; Hummelen, J. C.; Wudl, F.; Heeger, A. J. Polymer Photovoltaic Cells—Enhanced Efficiencies via a Network of Internal Donor−Acceptor Heterojunctions. *Science* **1995**, *270* (5243), 1789−1791.

(2) Li, G.; Shrotriya, V.; Huang, J. S.; Yao, Y.; Moriarty, T.; Emery, K.; Yang, Y. High-Efficiency Solution Processable Polymer Photovoltaic Cells by Self-Organization of Polymer Blends. *Nat. Mater.* **2005**, *4* (11), 864−868.

(3) Peet, J.; Kim, J. Y.; Coates, N. E.; Ma, W. L.; Moses, D.; Heeger, A. J.; Bazan, G. C. Efficiency Enhancement in Low-Bandgap Polymer Solar Cells by Processing with Alkane Dithiols. *Nat. Mater.* **2007**, *6* (7), 497−500.

(4) Kim, J. Y.; Lee, K.; Coates, N. E.; Moses, D.; Nguyen, T. Q.; Dante, M.; Heeger, A. J. Efficient Tandem Polymer Solar Cells Fabricated by All-Solution Processing. *Science* **2007**, *317* (5835), 222−225.

(5) Brabec, C. J.; Sariciftci, N. S.; Hummelen, J. C. Plastic Solar Cells. *Adv. Funct. Mater.* **2001**, *11* (1), 15−26.

(6) Günes, S.; Neugebauer, H.; Sariciftci, N. S. Conjugated Polymer-Based Organic Solar Cells. *Chem. Rev.* **2007**, *107* (4), 1324−1338.

(7) Li, G.; Zhu, R.; Yang, Y. Polymer Solar Cells. *Nat. Photonics* **2012**, *6* (3), 153−161.

(8) Zhou, H. X.; Yang, L. Q.; You, W. Rational Design of High Performance Conjugated Polymers for Organic Solar Cells. *Macromolecules* **2012**, *45* (2), 607−632.

(9) Dou, L. T.; You, J. B.; Yang, J.; Chen, C. C.; He, Y. J.; Murase, S.; Moriarty, T.; Emery, K.; Li, G.; Yang, Y. Tandem Polymer Solar Cells Featuring a Spectrally Matched Low-Bandgap Polymer. *Nat. Photonics* **2012**, *6* (3), 180−185.

(10) Svensson, M.; Zhang, F. L.; Veenstra, S. C.; Verhees, W. J. H.; Hummelen, J. C.; Kroon, J. M.; Inganäs, O.; Andersson, M. R. High-Performance Polymer Solar Cells of an Alternating Polyfluorene Copolymer and a Fullerene Derivative. *Adv. Mater.* **2003**, *15* (12), 988−991.

(11) Coffin, R. C.; Peet, J.; Rogers, J.; Bazan, G. C. Streamlined Microwave-Assisted Preparation of Narrow-Bandgap Conjugated Polymers for High-Performance Bulk Heterojunction Solar Cells. *Nat. Chem.* **2009**, *1* (8), 657−661.

(12) Park, S. H.; Roy, A.; Beaupré, S.; Cho, S.; Coates, N.; Moon, J. S.; Moses, D.; Leclerc, M.; Lee, K.; Heeger, A. J. Bulk Heterojunction Solar Cells with Internal Quantum Efficiency Approaching 100%. *Nat. Photonics* **2009**, *3* (5), 297−302.

(13) Amb, C. M.; Chen, S.; Graham, K. R.; Subbiah, J.; Small, C. E.; So, F.; Reynolds, J. R. Dithienogermole as a Fused Electron Donor in Bulk Heterojunction Solar Cells. *J. Am. Chem. Soc.* **2011**, *133* (26), 10062−10065.

(14) Chu, T.-Y.; Lu, J.; Beaupré, S.; Zhang, Y.; Pouliot, J.-R.; Wakim, S.; Zhou, J.; Leclerc, M.; Li, Z.; Ding, J.; Tao, Y. Bulk Heterojunction Solar Cells Using Thieno[3,4-*c*]Pyrrole-4,6-Dione and Dithieno[3,2-*b*:2′,3′-*d*]Silole Copolymer with a Power Conversion Efficiency of 7.3%. *J. Am. Chem. Soc.* **2011**, *133* (12), 4250−4253.

(15) Alem, S.; Chu, T. Y.; Tse, S. C.; Wakim, S.; Lu, J. P.; Movileanu, R.; Tao, Y.; Bélanger, F.; Désilets, D.; Beaupré, S.; Leclerc, M.; Rodman, S.; Waller, D.; Gaudiana, R. Effect of Mixed Solvents on

PCDTBT:PC70BM-Based Solar Cells. *Org. Electron.* **2011**, *12* (11), 1788−1793.
(16) Blouin, N.; Michaud, A.; Gendron, D.; Wakim, S.; Blair, E.; Neagu-Plesu, R.; Belletête, M.; Durocher, G.; Tao, Y.; Leclerc, M. Toward a Rational Design of Poly(2,7-Carbazole) Derivatives for Solar Cells. *J. Am. Chem. Soc.* **2008**, *130* (2), 732−742.
(17) Cho, S.; Seo, J. H.; Park, S. H.; Beaupré, S.; Leclerc, M.; Heeger, A. J. A Thermally Stable Semiconducting Polymer. *Adv. Mater.* **2010**, *22* (11), 1253−1257.
(18) Blouin, N.; Michaud, A.; Leclerc, M. A Low-Bandgap Poly(2,7-Carbazole) Derivative for Use in High-Performance Solar Cells. *Adv. Mater.* **2007**, *19* (17), 2295−2300.
(19) Cheedarala, R. K.; Kim, G. H.; Cho, S.; Lee, J.; Kim, J.; Song, H. K.; Kim, J. Y.; Yang, C. Ladder-Type Heteroacene Polymers Bearing Carbazole and Thiophene Ring Units and Their Use in Field-Effect Transistors and Photovoltaic Cells. *J. Mater. Chem.* **2011**, *21* (3), 843−850.
(20) Kim, B.; Yeom, H. R.; Yun, M. H.; Kim, J. Y.; Yang, C. A Selenophene Analogue of PCDTBT: Selective Fine-Tuning of Lumo to Lower of the Bandgap for Efficient Polymer Solar Cells. *Macromolecules* **2012**, *45* (21), 8658−8664.
(21) Kim, J.; Yun, M. H.; Kim, G. H.; Kim, J. Y.; Yang, C. Replacing 2,1,3-Benzothiadiazole with 2,1,3-Naphthothiadiazole in PCDTBT: Towards a Low Bandgap Polymer with Deep Homo Energy Level. *Polym. Chem.* **2012**, *3* (12), 3276−3281.
(22) Tumbleston, J. R.; Stuart, A. C.; Gann, E.; You, W.; Ade, H. Fluorinated Polymer Yields High Organic Solar Cell Performance for a Wide Range of Morphologies. *Adv. Funct. Mater.* **2013**, *23* (27), 3463−3470.
(23) Stuart, A. C.; Tumbleston, J. R.; Zhou, H.; Li, W.; Liu, S.; Ade, H.; You, W. Fluorine Substituents Reduce Charge Recombination and Drive Structure and Morphology Development in Polymer Solar Cells. *J. Am. Chem. Soc.* **2013**, *135* (5), 1806−1815.
(24) Schroeder, B. C.; Ashraf, R. S.; Thomas, S.; White, A. J. P.; Biniek, L.; Nielsen, C. B.; Zhang, W. M.; Huang, Z. G.; Tuladhar, P. S.; Watkins, S. E.; Anthopoulos, T. D.; Durrant, J. R.; McCulloch, I. Synthesis of Novel Thieno 3,2-*b*-Thienobis(Silolothiophene)-Based Low Bandgap Polymers for Organic Photovoltaics. *Chem. Commun.* **2012**, *48* (62), 7699−7701.
(25) Schroeder, B. C.; Huang, Z. G.; Ashraf, R. S.; Smith, J.; D'Angelo, P.; Watkins, S. E.; Anthopoulos, T. D.; Durrant, J. R.; McCulloch, I. Silaindacenodithiophene-Based Low Band Gap Polymers—The Effect of Fluorine Substitution on Device Performances and Film Morphologies. *Adv. Funct. Mater.* **2012**, *22* (8), 1663−1670.
(26) Chen, H. Y.; Hou, J. H.; Zhang, S. Q.; Liang, Y. Y.; Yang, G. W.; Yang, Y.; Yu, L. P.; Wu, Y.; Li, G. Polymer Solar Cells with Enhanced Open-Circuit Voltage and Efficiency. *Nat. Photonics* **2009**, *3* (11), 649−653.
(27) Li, Z.; Lu, J. P.; Tse, S. C.; Zhou, J. Y.; Du, X. M.; Tao, Y.; Ding, J. F. Synthesis and Applications of Difluorobenzothiadiazole Based Conjugated Polymers for Organic Photovoltaics. *J. Mater. Chem.* **2011**, *21* (9), 3226−3233.
(28) Liang, Y. Y.; Xu, Z.; Xia, J. B.; Tsai, S. T.; Wu, Y.; Li, G.; Ray, C.; Yu, L. P. For the Bright Future-Bulk Heterojunction Polymer Solar Cells with Power Conversion Efficiency of 7.4%. *Adv. Mater.* **2010**, *22* (20), E135−E138.
(29) Son, H. J.; Wang, W.; Xu, T.; Liang, Y. Y.; Wu, Y. E.; Li, G.; Yu, L. P. Synthesis of Fluorinated Polythienothiophene-Co-Benzodithiophenes and Effect of Fluorination on the Photovoltaic Properties. *J. Am. Chem. Soc.* **2011**, *133* (6), 1885−1894.
(30) Price, S. C.; Stuart, A. C.; Yang, L. Q.; Zhou, H. X.; You, W. Fluorine Substituted Conjugated Polymer of Medium Band Gap Yields 7% Efficiency in Polymer−Fullerene Solar Cells. *J. Am. Chem. Soc.* **2011**, *133* (12), 4625−4631.
(31) Zhang, Y.; Chien, S. C.; Chen, K. S.; Yip, H. L.; Sun, Y.; Davies, J. A.; Chen, F. C.; Jen, A. K. Y. Increased Open Circuit Voltage in Fluorinated Benzothiadiazole-Based Alternating Conjugated Polymers. *Chem. Commun.* **2011**, *47* (39), 11026−11028.
(32) Zhang, Y.; Zou, J. Y.; Cheuh, C. C.; Yip, H. L.; Jen, A. K. Y. Significant Improved Performance of Photovoltaic Cells Made from a Partially Fluorinated Cyclopentadithiophene/Benzothiadiazole Conjugated Polymer. *Macromolecules* **2012**, *45* (13), 5427−5435.
(33) Albrecht, S.; Janietz, S.; Schindler, W.; Frisch, J.; Kurpiers, J.; Kniepert, J.; Inal, S.; Pingel, P.; Fostiropoulos, K.; Koch, N.; Neher, D. Fluorinated Copolymer Pcpdtbt with Enhanced Open-Circuit Voltage and Reduced Recombination for Highly Efficient Polymer Solar Cells. *J. Am. Chem. Soc.* **2012**, *134* (36), 14932−14944.
(34) Zhou, H. X.; Yang, L. Q.; Stuart, A. C.; Price, S. C.; Liu, S. B.; You, W. Development of Fluorinated Benzothiadiazole as a Structural Unit for a Polymer Solar Cell of 7% Efficiency. *Angew. Chem., Int. Ed.* **2011**, *50* (13), 2995−2998.
(35) Yang, L. Q.; Tumbleston, J. R.; Zhou, H. X.; Ade, H.; You, W. Disentangling the Impact of Side Chains and Fluorine Substituents of Conjugated Donor Polymers on the Performance of Photovoltaic Blends. *Energy Environ. Sci.* **2013**, *6* (1), 316−326.
(36) Rolczynski, B. S.; Szarko, J. M.; Son, H. J.; Liang, Y. Y.; Yu, L. P.; Chen, L. X. Ultrafast Intramolecular Exciton Splitting Dynamics in Isolated Low-Band-gap Polymers and Their Implication in Photovoltaic Materials Design. *J. Am. Chem. Soc.* **2012**, *134* (9), 4142−4152.
(37) van der Poll, T. S.; Love, J. A.; Nguyen, T.-Q.; Bazan, G. C. Non-Basic High-Performance Molecules for Solution-Processed Organic Solar Cells. *Adv. Mater.* **2012**, *24* (27), 3646−3649.
(38) Cho, N.; Song, K.; Lee, J. K.; Ko, J. Facile Synthesis of Fluorine-Substituted Benzothiadiazole-Based Organic Semiconductors and Their Use in Solution-Processed Small-Molecule Organic Solar Cells. *Chem.—Eur. J.* **2012**, *18* (36), 11433−11439.
(39) Yang, C.; Orfino, F. P.; Holdcroft, S. A Phenomenological Model for Predicting Thermochromism of Regioregular and Non-regioregular Poly(3-Alkylthiophenes). *Macromolecules* **1996**, *29* (20), 6510−6517.
(40) Sakamoto, Y.; Komatsu, S.; Suzuki, T. Tetradecafluorosexithiophene: The First Perfluorinated Oligothiophene. *J. Am. Chem. Soc.* **2001**, *123* (19), 4643−4644.
(41) Bronstein, H.; Frost, J. M.; Hadipour, A.; Kim, Y.; Nielsen, C. B.; Ashraf, R. S.; Rand, B. P.; Watkins, S.; McCulloch, I. Effect of Fluorination on the Properties of a Donor-Acceptor Copolymer for use in Photovoltaic Cells and Transistors. *Chem. Mater.* **2013**, *25* (3), 277−285.
(42) Carsten, B.; Szarko, J. M.; Son, H. J.; Wang, W.; Lu, L. Y.; He, F.; Rolczynski, B. S.; Lou, S. J.; Chen, L. X.; Yu, L. P. Examining the Effect of the Dipole Moment on Charge Separation in Donor−Acceptor Polymers for Organic Photovoltaic Applications. *J. Am. Chem. Soc.* **2011**, *133* (50), 20468−20475.
(43) Carsten, B.; Szarko, J. M.; Lu, L. Y.; Son, H. J.; He, F.; Botros, Y. Y.; Chen, L. X.; Yu, L. P. Mediating Solar Cell Performance by Controlling The Internal Dipole Change in Organic Photovoltaic Polymers. *Macromolecules* **2012**, *45* (16), 6390−6395.
(44) Chu, T. Y.; Alem, S.; Tsang, S. W.; Tse, S. C.; Wakim, S.; Lu, J. P.; Dennler, G.; Waller, D.; Gaudiana, R.; Tao, Y. Morphology Control in Polycarbazole Based Bulk Heterojunction Solar Cells and Its Impact on Device Performance. *Appl. Phys. Lett.* **2011**, *98*, No. 253301.
(45) Liu, X.; Wen, W.; Bazan, G. C. Post-Deposition Treatment of an Arylated-Carbazole Conjugated Polymer for Solar Cell Fabrication. *Adv. Mater.* **2012**, *24* (33), 4505−4510.
(46) Alghamdi, A. A.; Watters, D. C.; Yi, H.; Al-Faifi, S.; Almeataq, M. S.; Coles, D.; Kingsley, J.; Lidzey, D. G.; Iraqi, A. Selenophene vs. Thiophene in Benzothiadiazole-based Low Energy gap Donor−Acceptor Polymers for Photovoltaic Applications. *J. Mater. Chem. A* **2013**, *1* (16), 5165−5171.
(47) Yi, H.; Al-Faifi, S.; Iraqi, A.; Watters, D. C.; Kingsley, J.; Lidzey, D. G. Carbazole and Thienyl Benzo [1, 2, 5] Thiadiazole Based Polymers with Improved Open Circuit Voltages and Processability for Application in Solar Cells. *J. Mater. Chem.* **2011**, *21* (35), 13649−13656.
(48) Minnaert, B.; Burgelman, M. *Prog. Photovolt.* **2007**, *15*, 741−748.

(49) Sze, S. M. *Physics of Semiconductor Devices*; Wiley: New York, 1969.
(50) Wetzelaer, G.; Kuik, M.; Lenes, M.; Blom, P. Origin of the Dark-Current Ideality Factor in Polymer: Fullerene Bulk Heterojunction Solar Cells. *Appl. Phys. Lett.* **2011**, *99* (15), No. 153506.
(51) Street, R.; Schoendorf, M.; Roy, A.; Lee, J. Interface State Recombination in Organic Solar Cells. *Phys. Rev. B* **2010**, *81* (20), 205307.
(52) Kirchartz, T.; Pieters, B. E.; Kirkpatrick, J.; Rau, U.; Nelson, J. Recombination via Tail States in Polythiophene: Fullerene Solar Cells. *Phys. Rev. B* **2011**, *83* (11), No. 115209.
(53) Soldera, M.; Taretto, K.; Kirchartz, T. Comparison of Device Models for Organic Solar Cells: Band-to-Band Vs. Tail States Recombination. *Phys. Status Solidi A* **2012**, *209* (1), 207−215.
(54) Namkoong, G.; Kong, J.; Samson, M.; Hwang, I. W.; Lee, K. Active Layer Thickness Effect on the Recombination Process of PCDTBT: PC71BM Organic Solar Cells. *Org. Electron.* **2013**, *14* (1), 74−79.
(55) Potscavage, W. J.; Sharma, A.; Kippelen, B. Critical Interfaces in Organic Solar Cells and Their Influence on the Open-Circuit Voltage. *Acc. Chem. Res.* **2009**, *42* (11), 1758−1767.
(56) Moliton, A.; Nunzi, J. M. How to Model the Behaviour of Organic Photovoltaic Cells. *Polym. Int.* **2006**, *55* (6), 583−600.
(57) Vandewal, K.; Tvingstedt, K.; Gadisa, A.; Inganäs, O.; Manca, J. V. On the Origin of the Open-Circuit Voltage of Polymer-Fullerene Solar Cells. *Nat. Mater.* **2009**, *8* (11), 904−909.
(58) Maurano, A.; Hamilton, R.; Shuttle, C. G.; Ballantyne, A. M.; Nelson, J.; O'Regan, B.; Zhang, W. M.; McCulloch, I.; Azimi, H.; Morana, M.; Brabec, C. J.; Durrant, J. R. Recombination Dynamics as a Key Determinant of Open Circuit Voltage in Organic Bulk Heterojunction Solar Cells: A Comparison of Four Different Donor Polymers. *Adv. Mater.* **2010**, *22* (44), 4987−4992.
(59) Shuttle, C. G.; O'Regan, B.; Ballantyne, A. M.; Nelson, J.; Bradley, D. D. C.; Durrant, J. R. Bimolecular Recombination Losses in Polythiophene: Fullerene Solar Cells. *Phys. Rev. B* **2008**, *78*, 113201.
(60) Nelson, J.; Kirkpatrick, J.; Ravirajan, P. Factors Limiting the Efficiency of Molecular Photovoltaic Devices. *Phys. Rev. B* **2004**, *69*, No. 35337.
(61) Kim, Y.; Cook, S.; Tuladhar, S. M.; Choulis, S. A.; Nelson, J.; Durrant, J. R.; Bradley, D. D. C.; Giles, M.; McCulloch, I.; Ha, C. S.; Ree, M. A Strong Regioregularity Effect in Self-Organizing Conjugated Polymer Films and High-Efficiency Polythiophene: Fullerene Solar Cells. *Nat. Mater.* **2006**, *5* (3), 197−203.
(62) Huang, J.; Zhao, Y.; He, W.; Jia, H.; Lu, Z.; Jiang, B.; Zhan, C.; Pei, Q.; Liu, Y.; Yao, J. Effects of Structure-Manipulated Molecular Stacking on Solid-State Optical Properties and Device Performances. *Polym. Chem.* **2012**, *3* (10), 2832−2841.
(63) Tang, A.; Li, L.; Lu, Z.; Huang, J.; Jia, H.; Zhan, C.; Tan, Z. a.; Li, Y.; Yao, J. Significant Improvement of Photovoltaic Performance by Embedding Thiophene in Solution-Processed Star-Shaped TPA-DPP Backbone. *J. Mater. Chem. A* **2013**, *1* (18), 5747−5757.
(64) Wang, W.; Xu, W.; Cosimbescu, L.; Choi, D.; Li, L.; Yang, Z. Anthraquinone with Tailored Structure for a Nonaqueous Metal−Organic Redox Flow Battery. *Chem. Commun.* **2012**, *48* (53), 6669−6671.